PHYSICAL REVIEW B **84**, 140411(R) (2011)

Density-functional study of paramagnetic iron

Hualei Zhang,[1] Börje Johansson,[1,2] and Levente Vitos[1,2,3,*]

[1]*Applied Materials Physics, Department of Materials Science and Engineering, Royal Institute of Technology, Stockholm SE-100 44, Sweden*

[2]*Department of Physics and Materials Science, Uppsala University, P.O. Box 516, Uppsala SE-75120, Sweden*

[3]*Research Institute for Solid State Physics and Optics, P.O. Box 49, Budapest H-1525, Hungary*

(Received 5 September 2011; revised manuscript received 5 October 2011; published 31 October 2011)

By using density-functional theory in combination with the coherent-potential approximation and the disordered local magnetic moment picture, we demonstrate that the competing high-temperature cubic phases of paramagnetic Fe correspond to two distinct total energy minima in the tetragonal (Bain) configurational space. Both the face-centered-cubic (fcc) and the body-centered-cubic (bcc) lattices are dynamically stable, and at static conditions the fcc structure is found to be the thermodynamically stable phase. The theoretical bcc and fcc bulk parameters are in agreement with the experimental data. Due to the shallow energy minimum around the bcc structure, increasing temperature is predicted to stabilize the bcc (δ) phase against the fcc (γ) one.

DOI: 10.1103/PhysRevB.84.140411 PACS number(s): 75.50.Bb, 64.30.Ef, 71.15.Nc, 75.20.En

Owing to its structural strength and high abundance, iron is a major alloy component in modern industry. At ambient pressure, bulk Fe crystallizes in the bcc structure with a ferromagnetic (FM) state (ferrite, α-Fe). Above the Curie temperature ($T_C = 1043$ K), it first adopts the paramagnetic (PM) bcc structure and then at 1183 K transforms to the PM fcc structure (austenite, γ-Fe). The austenite is stable between 1183 and 1667 K, above which the PM bcc structure (δ-Fe) is restabilized. Iron melts from the δ phase at 1811 K.

The technological importance placed Fe and its alloys (including steels) in the focus of scientific research. In spite of numerous theoretical efforts, however, the properties of the high-temperature phases of Fe and the mechanisms of the phase transformations have not yet been fully understood. Former investigations[1–6] argued that vibrational and magnetic contributions to the free energy are the possible driving forces behind the structural phase transitions in Fe. Recent density-functional theory (DFT) and dynamical mean-field theory (DMFT) studies[4,6,7] suggested that the magnetic energy is responsible for the survival of the α phase above T_C, and that γ-Fe is stabilized as a result of diminishing magnetic correlations with increasing temperature. Although the DFT-DMFT study gives clear evidence for the crucial role of the magnetic energy in the α-γ phase transition, it fails to account for the vibrational effects and thus explain the reentrance into the bcc phase before melting. In particular, the DFT-DMFT calculation using a quantum Monte Carlo (QMC) solver[6] predicts (i) increasing stability of the bcc lattice with temperature (with respect to the fcc lattice), (ii) fcc-bcc structural energy difference converging toward that obtained from 0 K nonmagnetic calculations, and (iii) mechanically unstable bcc structure at high temperature ($T > 1.3T_C$). As a matter of fact, the latter finding is in line with DFT calculations employing supercells to model the paramagnetic state.[4]

In this Rapid Communication, we put forward a DFT description of paramagnetic Fe, shedding light on the peculiar γ-δ structural change. In DFT studies, the completely random PM state may be described by the disordered local magnetic moment (DLM) picture.[8] Since the magnetic short-range correlations become negligible well above the transition temperature,[5,6] the DLM model, in combination with the coherent potential approximation (CPA),[9,10] is expected to correctly account for the random distribution of the local magnetic moments in the PM state.[11–13] Here we use the exact muffin-tin orbitals method[14,15] within the generalized gradient approximation[16] and the DLM-CPA model to study the polymorphous bcc-fcc transformation in PM Fe. We adopt a two-parameter Bain scheme described by the volume (represented by the Wigner-Seitz radius w) and the tetragonal axial ratio (c/a). In order to investigate the mechanical stability and reveal the effect of phonon contribution to the free energy, we monitor the theoretical elastic parameters computed for the two PM cubic phases. We demonstrate that, in contrast to previous theoretical predictions,[4,6] both cubic phases of PM Fe are dynamically stable. Furthermore, at low temperatures the fcc phase is thermodynamically stable but the vibrational effects can stabilize the bcc phase before melting.

The total energy of PM Fe was calculated for Wigner-Seitz radii $2.40 \leqslant w/\text{bohr} \leqslant 2.75$ (with an interval of 0.025) and the tetragonal lattice parameter $0.8 \leqslant c/a \leqslant 1.65$ (with an interval of 0.05). For comparison, we also calculated the total energies of the nonmagnetic (NM) phase for $2.40 \leqslant w/\text{bohr} \leqslant 2.75$ and $0.8 \leqslant c/a \leqslant 1.65$. Within the DLM picture, PM Fe was described as a binary $\text{Fe}^{\uparrow}\text{Fe}^{\downarrow}$ alloy with an equal amount of spin-up ($\uparrow$) and spin-down ($\downarrow$) components. In a cubic lattice, there are three independent elastic constants C_{11}, C_{12}, and C_{44}, and they are connected to the tetragonal shear elastic constant $C' = (C_{11} - C_{12})/2$ and bulk modulus $B = (C_{11} + 2C_{12})/3$. Dynamical (mechanical) stability requires that $C_{44} > 0$, $C' > 0$, and $B > 0$. The numerical details of the calculations are described in Refs. 17–19. The accuracy of our approach may be assessed by comparing the present and former[20] theoretical results for FM Fe to the experimental data (Table I): The small discrepancies may be ascribed to the $\sim$1.0% underestimation of the experimental lattice parameter[21] by the gradient-level DFT.[16]

First, we compare the calculated Wigner-Seitz radii of PM Fe to the experimental data (Table I). At static conditions (0 K), w_{bcc} and w_{fcc} are 2.4% and 4.5% smaller than those measured[22] at 1189 and 1457 K, respectively. Moreover, the equilibrium DFT results give $(w_{\text{bcc}} - w_{\text{fcc}})/w_{\text{fcc}}|_{0\,\text{K}} = 1.84\%$, which is much larger than the QMC-DMFT[6] (0.77%) and

TABLE I. Theoretical equilibrium Wigner-Seitz radius w and lattice parameter a (bohrs), magnetic moment μ (μ_B), bulk modulus B and cubic shear elastic constants C' and C_{44} (GPa), Zener anisotropy ratio C_{44}/C', and elastic Debye temperature Θ (K) for ferromagnetic bcc and paramagnetic bcc and fcc Fe. The energy differences ΔE (mRy/atom) are relative to PM bcc Fe. DFT (1200 K) and DFT (1400 K) are the theoretical results obtained for Wigner-Seitz radii corresponding to 1200 and 1400 K, respectively (see the text). For comparison, former theoretical values (Refs. 6 and 20) and some experimental data (indicated by the corresponding temperature) (Refs. 21–24) are also shown.

System	Method	w	a	μ	B	C'	C_{44}	C_{44}/C'	Θ	ΔE
FM bcc	DFT	2.6405	5.3628	2.21	193.87	77.97	106.73	1.37	502	−6.80
	DFT[a]	2.6434	5.3687	2.17	186	69	99	1.43		
	4 K[b]	2.6680	5.4187	2.22	173.10	52.5	121.9	2.32		
PM bcc	DFT	2.6379	5.3575	2.20	172.49	17.86	153.82	8.61	431	0
	DFT(1200 K)	2.6837	5.4505	2.34	131.50	19.04	129.30	6.77	412	
	DMFT[c]	2.6825	5.4481	2.01	150					
	1189 K,[d] 1173 K[e]	2.7033[d]	5.4904[d]		131.07[e]	13.3[e]	99[e]	7.44[e]		
PM fcc	DFT	2.5893	6.6257	1.42	131.02	61.61	213.40	3.46	574	−3.11
	DFT (1400 K)	2.6757	6.8468	2.08	90.81	27.92	138.28	4.95	442	
	DMFT[c]	2.6621	6.8120	1.89	161					
	1457 K,[d] 1428 K[f]	2.7110[d]	6.9371[d]		132.67[f]	16[f]	77[f]	4.81[f]		

[a]Reference 20.
[b]Reference 21.
[c]Reference 6.
[d]Reference 22.
[e]Reference 23.
[f]Reference 24.

experimental[22] (0.34% at 1189 K) values. We note that the differences between the theoretical and experimental bulk parameters of fcc Fe are even larger in the case of DFT calculations performed for the NM state[20,25] (not shown).

At equilibrium, the present local magnetic moments differ by ∼9% for PM bcc Fe and by ∼25% for PM fcc Fe from those obtained in the QMC-DMFT simulation near the transition temperature.[6] The PM bcc lattice has a rather robust local magnetic moment as a function of w, but in the PM fcc lattice there is a magnetic transition at ∼2.55 bohrs (Fig. 1). The PM fcc energy minimum, located relatively close to this critical radius, is very shallow (compared to the PM bcc one) and thus the thermal expansion is expected to have a larger impact on the fcc lattice than on the bcc lattice. Indeed, the strongly volume-dependent magnetic pressure results in a significantly larger linear thermal expansion coefficient for fcc Fe [23.8×10^{-6} 1/K (Ref. 22)] than for bcc Fe [14.5×10^{-6} 1/K (Ref. 22)]. Correcting the theoretical results for the thermal expansion (assuming a linear thermal expansion), we find that the deviation between the theoretical and experimental Wigner-Seitz radii reduces to 0.7% for bcc at 1200 K and to 1.3% for fcc at 1400 K [DFT (1200 K) and DFT (1400 K), Table I]. Notice that for both theoretical radii the remaining error after the thermal expansion correction has been included is of the order of the DFT error. Around the α-γ transition temperature, we obtain $(w_{bcc} - w_{fcc})/w_{fcc}|_{1200\ K} = 0.76\%$, which is very close to that found in the QMC-DMFT calculation.[6]

The total energy versus c/a and w for NM Fe (lower panel, Fig. 2) has two local minima. The first one ($c/a = \sqrt{2}$) corresponds to the NM fcc phase and the second one ($c/a = 0.9$) to a NM tetragonal phase ($TET_{0.9}$). Around the NM bcc structure ($c/a = 1$) there is a saddle point in the energy map and thus this lattice is mechanically unstable. The NM fcc lattice is ∼19 mRy lower in energy than the NM bcc phase. All these findings are in both qualitative and quantitative agreement with former DFT calculations.[6,26] On the other hand, for PM Fe the total energy map exhibits a rather unique behavior (upper panel, Fig. 2). The two cubic structures correspond to two local minima in the configurational space with a clear barrier between them. To the best of our knowledge, the local minimum at approximately $c/a = 1$ in the PM total energy has not been seen earlier in the supercell calculation[4] nor in

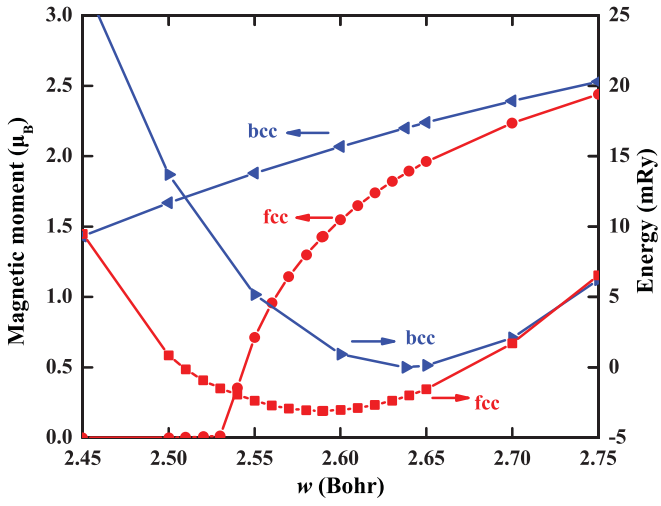

FIG. 1. (Color online) Left-hand axis: Local magnetic moments (in μ_B) for paramagnetic bcc (left triangles) and fcc (circles) Fe; right-hand axis: total energy (in mRy) for paramagnetic bcc (right triangles) and fcc (squares) Fe, plotted as a function of the Wigner-Seitz radius (w in bohrs). All energies are shown relative to the bcc energy minimum.

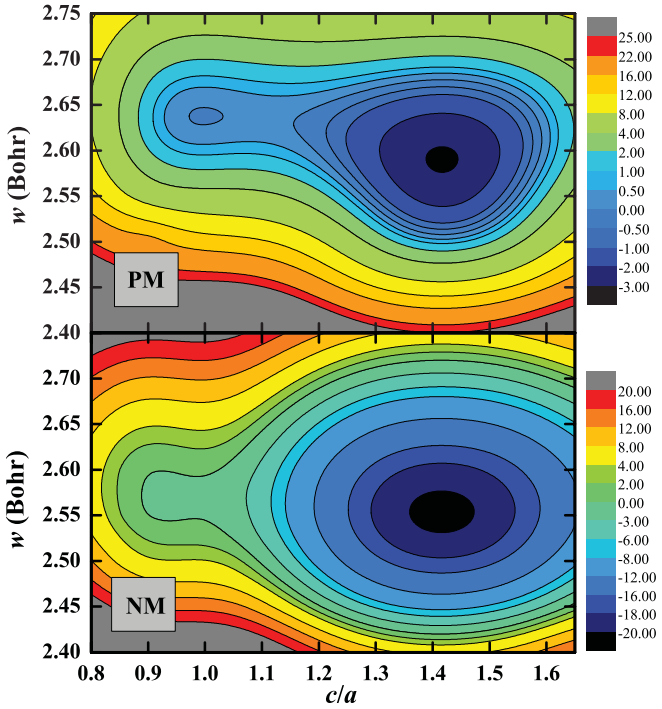

FIG. 2. (Color online) Total energy contour (in mRy) for paramagnetic (upper panel) and nonmagnetic (lower panel) Fe as a function of the tetragonal ratio (c/a) and the Wigner-Seitz radius (w in bohrs). The energies are plotted relative to the bcc ($c/a = 1$) minimum.

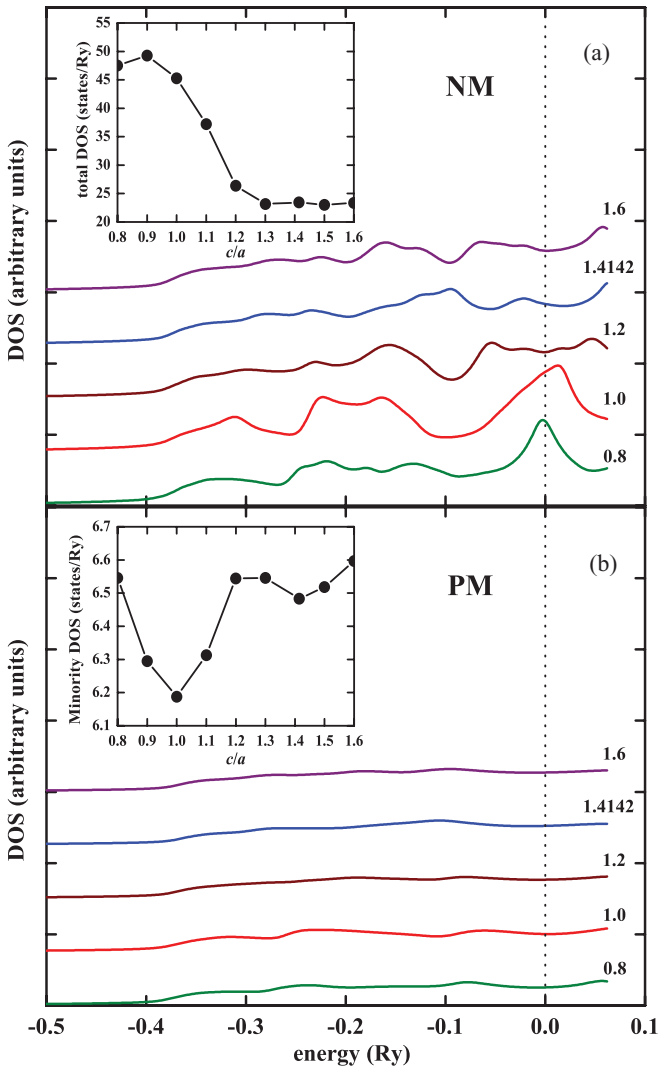

FIG. 3. (Color online) Density of states (arbitrary units) for nonmagnetic (a) and paramagnetic (b) Fe plotted as a function of energy relative to the Fermi level. The five curves correspond to five different tetragonal lattice parameters $c/a = 0.8, 1.0, 1.2, \sqrt{2}$, and 1.6. In the insets, the total [NM Fe, (a)] and the minority [PM Fe, (b)] density of states at the Fermi level are shown as a function of c/a.

the high-temperature QMC-DMFT simulation.[6] In contrast, these former studies predicted a low c/a (<1) PM tetragonal phase for high-temperature Fe, similar to the one seen for NM Fe (lower panel, Fig. 2). Our DLM-CPA calculation does not verify the existence of such a dynamically stable tetragonal lattice for PM Fe.

A second important feature of the PM energy map is the strong volume dependence of the structural energy difference. At equilibrium, the fcc lattice is ∼3.11 mRy below bcc. For the PM bcc-fcc energy difference, the supercell[4] and the high-temperature ($T \sim 3.6T_C$) QMC-DMFT[6] calculations gave ∼10 and ∼13 mRy, respectively, which are more than three times larger than our DLM-CPA result. Fixing the Wigner-Seitz radius to 2.50 bohrs increases the present structural energy difference to ∼12.8 mRy. However, for $w \gtrsim 2.70$ bohrs (see also Fig. 1) the two cubic lattices become nearly degenerate.

The fixed-volume distortions around the energy minimum can give useful information about the tetragonal elastic constant: C' represents the curvature of the total energy surface along constant w. Comparing the contour lines at approximately $c/a = 1$ and $c/a = \sqrt{2}$ (upper panel, Fig. 2), we see that the PM bcc phase has a shallower energy versus c/a minimum than the PM fcc phase. This is also confirmed by our calculated elastic constants (Table I).

In general, the present theoretical elastic constants obtained at the equilibrium volumes (DFT, Table I) are significantly larger than the measured values.[23,24] However, if we consider the results obtained for volumes corresponding to the experimental conditions [DFT (1200 K) and DFT (1400 K), Table I], the average deviation between the two sets of data drops to ∼30%. Theory is found to reproduce the unusually large anisotropy of PM Fe. In particular, the exceptionally large Zener anisotropy ratio of PM bcc Fe is due to the very low tetragonal elastic constant relative to that of FM bcc Fe. Namely, going from the 0 K FM to the high-temperature (1200 K) PM state reduces the theoretical C'_{bcc} by 76%, compared to 73% obtained in experiment.[23] Finally, it is important to note that the calculated B, C', and C_{44} satisfy the dynamical stability conditions for both PM cubic structures.

The elastically softer PM bcc phase, compared to the fcc one, is expected to have a larger phonon entropy and thus be stabilized by increasing temperature. To quantify this prediction, we consider the elastic Debye temperatures (Θ, Table I) obtained by averaging the longitudinal and transversal sound velocities calculated from the elastic constants.[27,28] The theoretical Debye temperature of PM bcc Fe is smaller than that of PM fcc Fe by 24.9% at equilibrium volumes and by

3.8% at volumes corresponding to 1667 K (i.e., Wigner-Seitz radii of 2.702 bohrs for bcc and 2.692 bohrs for fcc). Using the high-temperature expansion for the phonon free-energy difference between the two structures [$3k_BT(\Theta_{fcc} - \Theta_{bcc})/\Theta_{fcc}$, k_B is the Boltzmann constant],[29] in connection with the calculated structural energy difference and Debye temperatures, we find that ∼1580 K is needed to stabilize the completely random PM bcc phase against the PM fcc phase. It is gratifying that this simple theoretical prediction is rather close to the observed γ-δ transition temperature (1667 K). For a quantitative calculation, however, one should go beyond the present approximation and take into account the longitudinal spin fluctuations[30] and the magnetoelastic coupling.[31]

Monitoring the electronic density of states (DOS) for NM and PM Fe (Fig. 3) as a function of c/a (calculated for $w = 2.56$ bohrs for the NM state and $w = 2.62$ bohrs for the PM state) we can understand the stability of different phases. For NM Fe [Fig. 3(a)], there is a large peak in the DOS around the Fermi level (E_F) for $c/a \lesssim 1.1$, which gradually disappears at larger c/a ratios. This peak is in fact responsible for the dynamical instability of NM bcc Fe.[32] The situation is quite different for PM Fe [Fig. 3(b)]. For each c/a, the total PM DOS has a shallow local minimum around E_F and this minimum shows weak structure dependence. The minority PM and the NM DOS at E_F are shown in insets of Fig. 3 as a function of c/a. We note that according to the spin-resolved DOS (not shown), the minority states give ∼60% of the total PM DOS (E_F) and thus here we focus on that spin channel only. We find that the largest structure-induced change in PM DOS (E_F) is ∼0.4 states/Ry compared to ∼26 states/Ry obtained for NM DOS(E_F). The large drop in NM DOS (E_F) when going from low c/a to high c/a explains the stability of the NM fcc phase. On the other hand, the minority PM DOS (E_F) exhibits two local minima at approximately $c/a = 1$ and $c/a = \sqrt{2}$, making these structures stable along the Bain path. Figure 3 also demonstrates that the structural effects are much more delicate for PM Fe than for NM Fe, and only a very careful and accurate study can properly account for them.

Based on the present DFT and former QMC-DMFT results,[6] we propose a scenario for the structural transition sequence in Fe. At low temperature, magnetic correlations stabilize the α phase of Fe by ∼3.7–6.8 mRy relative to the paramagnetic phases. With increasing temperature, the correlation effects are gradually diminished but still survive above the magnetic transition, keeping the bcc structure stable up to ∼1183 K. Without this magnetic energy, the γ phase would be more stable at low temperatures. Around and above the α-γ transition temperature, the correlation is not large enough anymore to overcome the structural energy difference and thus the γ phase becomes stable. However, in the paramagnetic state, the bcc lattice is softer than the fcc lattice and as a consequence temperature restabilizes the bcc (δ) phase at ∼1667 K.

In summary, the excellent correspondence between the measured physical properties and those predicted in the present Rapid Communication demonstrates that DFT in combination with alloy theory suitably describes the magnetically disordered phases of Fe. Our DFT-DLM level results show that both cubic phases of paramagnetic Fe are dynamically stable. The transition in the paramagnetic state of the fcc phase explains the anomalous thermal expansion coefficient seen for this lattice, whereas the soft tetragonal mode of the bcc phase is shown to be responsible for the stabilization of the δ phase before melting.

The Swedish Research Council, the Swedish Energy Agency, the Swedish Steel Producers' Association, the European Research Council, the Hungarian Scientific Research Fund (research project OTKA 84078), and the China Scholarship Council are acknowledged for financial support.

*levente@kth.se

[1] R. J. Weiss and K. J. Tauer, Phys. Rev. **102**, 1490 (1956).
[2] L. Kaufman, E. V. Clougherty, and R. J. Weiss, Acta Metall. **11**, 323 (1963).
[3] H. Hasegawa and D. G. Pettifor, Phys. Rev. Lett. **50**, 130 (1983).
[4] S. V. Okatov, A. R. Kuznetsov, Y. N. Gornostyrev, V. N. Urtsev, and M. I. Katsnelson, Phys. Rev. B **79**, 094111 (2009).
[5] A. I. Lichtenstein, M. I. Katsnelson, and G. Kotliar, Phys. Rev. Lett. **87**, 067205 (2001).
[6] I. Leonov, A. I. Poteryaev, V. I. Anisimov, and D. Vollhardt, Phys. Rev. Lett. **106**, 106405 (2011).
[7] X. Tao, D. P. Landau, T. C. Schulthess, and G. M. Stocks, Phys. Rev. Lett. **95**, 087207 (2005).
[8] J. Staunton *et al.*, J. Magn. Magn. Mater. **45**, 15 (1984).
[9] P. Soven, Phys. Rev. **156**, 809 (1967).
[10] B. L. Györffy, Phys. Rev. B **5**, 2382 (1972).
[11] L. Vitos, P. A. Korzhavyi, and B. Johansson, Phys. Rev. Lett. **88**, 155501 (2002).
[12] L. Vitos, P. A. Korzhavyi, and B. Johansson, Phys. Rev. Lett. **96**, 117210 (2006).
[13] L. Vitos, P. A. Korzhavyi, and B. Johansson, Nat. Mater. **2**, 25 (2003).
[14] L. Vitos, Phys. Rev. B **64**, 014107 (2001).
[15] O. K. Andersen, O. Jepsen, and G. Krier, *Lectures on Methods of Electronic Structure Calculations* (World Scientific, Singapore, 1994).
[16] J. P. Perdew, K. Burke, and M. Ernzerhof, Phys. Rev. Lett. **77**, 3865 (1996).
[17] H. L. Zhang, B. Johansson, and L. Vitos, Phys. Rev. B **79**, 224201 (2009).
[18] H. L. Zhang, N. Al-Zoubi, B. Johansson, and L. Vitos, J. Appl. Phys. **110**, 073707 (2011).
[19] H. L. Zhang, S. Lu, M. P. J. Punkkinen, Q.-M. Hu, B. Johansson, and L. Vitos, Phys. Rev. B **82**, 132409 (2010).
[20] G. Y. Guo and H. H. Wang, Chin. J. Phys. (Taipei) **38**, 949 (2000).
[21] J. A. Rayne and B. S. Chandrasekhar, Phys. Rev. **122**, 1714 (1961).
[22] Z. S. Basinski, W. Hume-Rothery, and A. L. Sutton, Proc. R. Soc. London A **229**, 459 (1955).
[23] D. J. Dever, J. Appl. Phys. **43**, 3293 (1972).
[24] J. Zarestky and C. Stassis, Phys. Rev. B **35**, 4500 (1987).

[25]S. Fox and H. J. F. Jansen, Phys. Rev. B **53**, 5119 (1996).
[26]D. J. Singh, W. E. Pickett, and H. Krakauer, Phys. Rev. B **43**, 11628 (1991).
[27]B. Magyari-Köpe, G. Grimvall, and L. Vitos, Phys. Rev. B **66**, 064210 (2002).
[28]G. Grimvall, *Thermophysical Properties of Materials* (North-Holland, Amsterdam, 1999).
[29]G. Grimvall, Phys. Scr. **13**, 59 (1976).
[30]A. V. Ruban, S. Khmelevskyi, P. Mohn, and B. Johansson, Phys. Rev. B **75**, 054402 (2007).
[31]L. Vitos and B. Johansson, Phys. Rev. B **79**, 024415 (2009).
[32]K. Kádas, L. Vitos, B. Johansson, and R. Ahuja, Proc. Natl. Acad. Sci. USA **106**, 15560 (2009).